

# FLUCTUATIONS IN THE ALPHA-EFFECT AND GRAND SOLAR MINIMA

S. V. Olemskoy<sup>1</sup>, A. R. Choudhuri<sup>2</sup>, and L. L. Kitchatinov<sup>1,3\*</sup>

<sup>1</sup>*Institute of Solar-Terrestrial Physics, Lermontov Str. 126A, Irkutsk 664033, Russia*

<sup>2</sup>*Department of Physics, Indian Institute of Science, Bangalore-560012*

<sup>3</sup>*Pulkovo Astronomical Observatory, St. Petersburg 176140, Russia*

## ABSTRACT

Parameters of a special kind of  $\alpha$ -effect known in dynamo theory as the Babcock–Leighton mechanism are estimated using the data of sunspot catalogs. The estimates evidence the presence of the Babcock–Leighton  $\alpha$ -effect on the Sun. Fluctuations of the  $\alpha$ -effect are also estimated. The fluctuation amplitude appreciably exceeds the mean value, and the characteristic time for the fluctuations is comparable to the period of the solar rotation. Fluctuations with the parameters found are included in a numerical model for the solar dynamo. Computations show irregular changes in the amplitudes of the magnetic cycles on time scales of centuries and millennia. The calculated statistical characteristics of the grand solar minima and maxima agree with the data on solar activity over the Holocene.

DOI: 10.1134/S1063772913050065

arXiv:1305.2660v1 [astro-ph.SR] 13 May 2013

---

\*E-mail: kit@iszf.irk.ru

## 1. INTRODUCTION

The purpose of the present work is twofold. First, we attempt to estimate the parameters of the solar dynamo  $\alpha$ -effect from sunspot data. We then use the found parameters in a numerical model of the solar dynamo to reproduce the grand minima of solar activity.

Dynamo theory explains solar magnetic activity in terms of two main effects: toroidal field production from the global poloidal field by differential rotation (the  $\Omega$ -effect) and the inverse transformation of the toroidal field into the poloidal field by cyclonic flows (the  $\alpha$ -effect). The resulting mechanism for the field generation is called the  $\alpha\Omega$ -dynamo (see, for example, [1]).

Differential solar rotation varies slightly with time. There are only torsional oscillations with the 11-year period of the solar cycle and an amplitude of several m/s [2,3]. Therefore, the  $\Omega$ -effect is fairly regular. The presence of this effect on the sun is evidenced by the observed dependence of the cycle amplitudes on the strengths of the poloidal (polar) field at the preceding solar minima [4-6]. At the same time, there is no correlation between the amplitudes of the solar cycles and the poloidal fields at *following* solar minima. The reason is believed to be a significant randomness in the  $\alpha$ -effect [7]. The  $\alpha$ -effect on the sun and other convective stars is related to small-scale cyclonic motions. Various versions of this effect differ only in the origin of the corresponding small-scale flows. These can be either convective flows [8], or motions due to magnetic buoyancy [9,10]. The  $\alpha$ -effect associated with the buoyant rise of toroidal fields to the solar surface was named the Babcock–Leighton mechanism.

The Babcock–Leighton mechanism deserves special attention for two reasons. First, in contrast to other types of  $\alpha$ -effect, this mechanism does not suffer from catastrophic quenching due to the conservation of magnetic helicity [11,12]. Therefore, this type of  $\alpha$ -effect may dominate on the Sun. Second, parameters of the Babcock–Leighton mechanism can be estimated from the sunspot data [13,14]. Recent estimations for three solar cycles [15] evidence operation of this mechanism on the Sun. The analysis of this paper relies on longer data series. We estimate both the parameters of the Babcock–Leighton mechanism for individual solar cycles and fluctuations of these parameters with time.

Fluctuations of the  $\alpha$ -effect are important for the theory of the solar dynamo. The grand minima of solar activity can be interpreted in terms of these fluctuations. Observations reveal the alternations of "usual" 11-year cycles with grand solar minima, the

Maunder minimum being the best known example. Grand minima have also been detected on solar-type stars [16]. The most popular - though not the only known - theory of grand minima explains them by fluctuations of dynamo parameters, mainly by the fluctuations of the  $\alpha$ -effect (see, for example, [17 - 20]). The main difficulty in this explanation is that too strong fluctuations comparable or even exceeding the mean values are required. It is difficult to imagine such fluctuations for the  $\alpha$ -effect due to convective turbulence. There are likely several tens of global convective cells simultaneously on the sun [21]. The relative amplitude of the fluctuations is inversely proportional to the square root of the cells number, and must be below unity. We expect, however, the Babcock–Leighton mechanism to be free from this difficulty. This mechanism is related to solar active regions. Even at solar maxima, there are only a few active regions simultaneously on the Sun. Therefore, we expect fluctuations in the Babcock–Leighton mechanism to be comparable by the order of magnitude to its mean parameters.

In the next section, we estimate the parameters of the Babcock–Leighton mechanism and their fluctuations using sunspot data. Section 3 describes the dynamo model with a non-local  $\alpha$ -effect corresponding to the Babcock–Leighton mechanism. The model allows for fluctuations in the  $\alpha$ -effect whose amplitude is specified in accordance with our observations-based estimates. We discuss results of long-term computations covering about one thousand magnetic cycles. Section 4 formulates our main conclusions.

## 2. ESTIMATING THE BABCOCK-LEIGHTON MECHANISM FROM SUNSPOT DATA

### *2.1. Method*

The Babcock–Leighton mechanism is related to Joy’s law for solar active regions. The law states that the leading spots (in the rotational motion) of bipolar groups are, on average, located closer to the equator than the trailing spots. Thus, on average, the line connecting the centers of opposite polarities displays a (positive) tilt to the solar lines of latitude (Fig. 1). The mean tilt angle  $\alpha$  increases with latitude, as must be the case if Joy’s law is due to the Coriolis force influence on the emerging magnetic loops [22].

Due to the finite tilt  $\alpha$ , the magnetic fields of active regions possess a poloidal component. Upon the decay of active regions and subsequent turbulent diffusion, this component

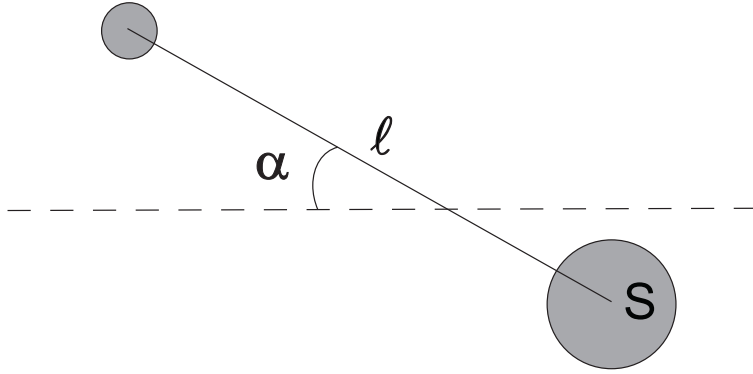


Fig. 1. Illustration of Joy's law and parameters of Eq.(1). The tilt angle  $\alpha$  is on average positive,  $l$  is the distance between the centers of opposite polarities and  $S$  is the area of the largest spot of the group. Northern hemisphere, the pole is upward.

contributes to the global poloidal field of the sun. We assume that the total contribution of active regions to the poloidal field made over a certain interval of a solar cycle can be estimated as

$$B = \sum_i S_i \ell_i \sin \alpha_i, \quad (1)$$

where  $S_i$  is the area of the largest spot of the group,  $\ell_i$  is the distance between the centers of opposite polarities, and  $\alpha_i$  is the tilt angle of the group axis to the East–West direction (see Fig. 1). The summed quantities are taken at the instant of maximum development of the sunspot group, and the contribution of each group to the sum (1) is taken once.

The estimation assumes that the contribution to the poloidal field is proportional to the magnetic flux of the active region. Since the magnetic fields of mature sunspots vary within a comparatively narrow interval from about 2.5 to 3.5 kG [23], we can assume the magnetic flux to be proportional to the area of the largest spot. Typical distances between the spots of a group are small compared to the solar radius. Turbulent diffusion will annihilate opposite polarities as the group decays. Only a minor part of the magnetic flux of an active region contributes to the global poloidal field. Babcock estimated this part by about 1% [9]. We expect this contribution to increase with  $\ell$ . Since  $\ell$  is small compared to  $R_\odot$ , we assume linear dependence on  $\ell$  in the sum (1). Finally, the poloidal field components of active regions are proportional to  $\sin \alpha$ .

When the summation in (1) is made over the entire solar cycle, we designate the resulting  $B$  value as  $B_{\text{cyc}}$ . Some evidence has been found earlier [15] that the relation between  $B_{\text{cyc}}$  and the poloidal field at the following activity minima is close to linear dependence. This indicates in favour of the action of the Babcock–Leighton mechanism on the

Sun. We are also interested in fluctuations in this mechanism, and so calculate the sums (1) for shorter time intervals. The lifetimes of most sunspots do not exceed one solar rotation. Therefore, the characteristic time of fluctuations in the Babcock–Leighton mechanism should not be longer than one solar rotation. However, it does not seem reasonable to calculate  $B$  of (1) for times shorter than one Carrington rotation. We designate the  $B$  values for individual solar rotations as  $B_{\text{Car}}$ . These values show significant fluctuations. Of course, the sum of all the  $B_{\text{Car}}$  values for the individual solar cycles equal  $B_{\text{cyc}}$ . The running average  $\langle B_{\text{Car}} \rangle$  over 13 rotations (approximately one year) varies smoothly with time, and shows no significant fluctuations. The relative deviation from this running mean for individual rotations is

$$B'_{\text{Car}} = \frac{B_{\text{Car}}}{\langle B_{\text{Car}} \rangle} - 1, \quad (2)$$

while the relative amplitude of the fluctuations is

$$\sigma_{B_{\text{Car}}} = \sqrt{\frac{\sum (B'_{\text{Car}})^2}{N}}, \quad (3)$$

where the summation is made over all  $N$  rotations presented in the sunspot catalog.

## 2.2. Data

Values of  $B_{\text{cyc}}$  were calculated earlier [15] for solar cycles 19–21 using the Catalog of Solar Activity (CSA) of the Pulkovo Observatory [24] ([http://www.gao.spb.ru/database/csa/groups\\_e.html](http://www.gao.spb.ru/database/csa/groups_e.html)). It was found that the relationship between the  $B_{\text{cyc}}$  for individual solar cycles and the amplitude of the poloidal field at the following solar minima is close to linear dependence. Here, we use the CSA data to estimate the fluctuations (2) and (3). Longer series of data are provided by the Kodaikanal (KK) and Mount Wilson (MW) observatories. The data comprising eight and six solar cycles, respectively, were digitized by Howard et al. [25,26] using the same technique ([ftp://ftp.ngdc.noaa.gov/STP/SOLAR\\_DATA/SUNSPOT\\_REGIONS](ftp://ftp.ngdc.noaa.gov/STP/SOLAR_DATA/SUNSPOT_REGIONS)). The digitizing technique [25,26] was aimed at using sunspots as tracers for measuring rotation and meridional flow. Therefore, the digitized KK and MW catalogs consist of pairs of datasets on sunspot groups observed on two consecutive days. We wish to reconstruct the evolution of the active regions from separate pairs of datasets. Each pair of observations contains information on a sunspot group observed on the first and second day. If separate pairs of datasets correspond to the same active region, the data for the second day of the preceding pair will coincide with the data

for the first day of the succeeding pair. Accordingly, the evolution of the sunspot groups was reconstructed by comparing the dates of observations and the morphological features of the active regions (group areas, numbers of spots, group coordinates, etc) for the second day of the preceding and the first day of following pairs of datasets.

Using this method, however, the same sunspot group may be included twice or even more times in the reconstructed data, if the initial KK and MW data have gaps. On the other hand, if a group was never observed during two successive days, this group would be lost in the reconstructed data. To assess possible multiple inclusions or losses of some groups, we compared the total number of sunspot groups in the reconstructed data with their number in the catalog of the Royal Greenwich Observatory (RGO) for the corresponding period of time (Table 1). The initial MW and KK catalogs contain data on sunspot groups located within  $\pm 60^\circ$  of the central meridian of the solar disk and observed on at least two days. We applied the same restriction when calculating the number of sunspot groups in the RGO catalog. The differences in the numbers of sunspot groups of about 200 for a total number of groups of about 15 000 are relatively small.

Table 1. Total number of sunspot groups based on KK, MW, and GRO data for corresponding observation intervals

Years	Numbers of sunspot groups in catalogs		
	RGO	KK	MW
1906–1987	16195	15990	–
1917–1985	14696	–	14552

The reconstructed data of the KK and MW catalogs enabled us to follow the evolution of sunspot groups and to estimate the sought for parameters of the Babcock–Leighton mechanism for most of the mature active regions. These catalogs also contain the data on the spot numbers in groups, their areas, coordinates, tilt angles, information on the leading and following parts of the groups, etc. The KK data cover the solar cycles 14-21, and MW data - cycles 16-21.

### 2.3. Results

Figure 2 shows the positions of individual solar cycles on a coordinate plane of the index  $A$  of the large-scale field for the solar minima succeeding these cycles versus  $B_{cyc}$  calculated with Eq. (1). The  $A$ -index estimates the amplitude of the large-scale magnetic field [4] (poloidal field for the epochs of solar minima).

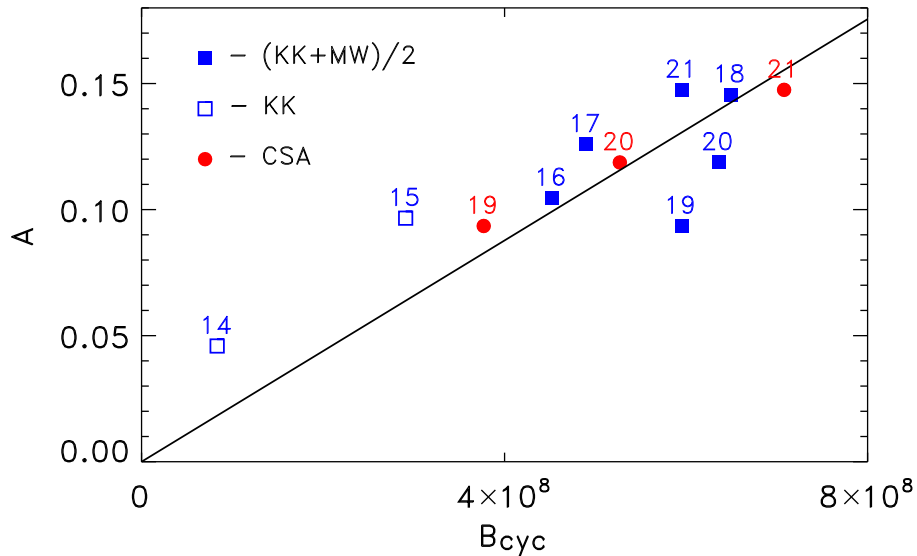


Fig. 2. Positions of individual solar cycles on the coordinate plane of  $B_{cyc}$  and  $A$ -index of large-scale magnetic field for solar minima succeeding these cycles. The numbers near the points show the cycles No.

The KK and MW catalogs give the areas of the spot umbrae, while the CSA presents the total areas including the penumbrae. Therefore, the CSA  $B_{cyc}$  values in Fig. 2 have been reduced by a factor of 0.2. A linear regression fit common for all the data,

$$A = 2.16 \times 10^{-10} B_{cyc}, \quad (4)$$

is also shown in Fig. 2. The KK and MW datasets are very similar. Common data points are therefore shown for solar cycles 16-21, for which KK and MW datasets overlap. When calculating  $B_{cyc}$  using (1),  $\ell_i$  was taken in kilometers and  $S_i$  in millionths of a solar hemisphere. The coefficients  $a$  of the linear fits,  $A = aB_{cyc}$ , for individual datasets, the correlation coefficients and relative amplitude of the fluctuations  $\sigma_{B_{Car}}$  (3) for CSA data are given in Table 2.

Table 2. Correlation coefficients  $R(B_{cyc}, A)$ , coefficients of linear regression  $a$ , and standard deviation  $\sigma_{B_{Car}}$  (3) calculated for the KK, MW, and CSA data

Parameters	CSA	KK	MW
$R(B_{cyc}, A)$	0.98	0.81	0.46
$a$	$2.20 \times 10^{-10}$	$2.06 \times 10^{-10}$	$2.17 \times 10^{-10}$
$\sigma_{B_{Car}}$	2.67		

There is a well known correlation between the index  $A$  for solar minima and the amplitudes of the succeeding solar cycles [4-6]. The differential rotation transforming the poloidal field into the toroidal field varies only weakly with time, and does not contain

significant random fluctuations. Therefore, there is a functional relation between the poloidal field at the solar minimum and the toroidal field at the following maximum (the sunspot activity is associated with the solar toroidal field). At the same time, there is no functional relationship between the cycle amplitude and the  $A$ -index of the following solar minimum [5,27]. Randomness in the  $\alpha$ -effect providing such a relation may be the explanation for its lack of prominence. This, however, does not preclude estimating the contribution of the  $\alpha$ -effect to the poloidal field generation, including all the inherent fluctuations. Formula (1) provides such an estimate for the special case of the  $\alpha$ -effect named the Babcock–Leighton mechanism. The estimated  $B_{cyc}$  correlate well with the  $A$ -index. Figure 2 and Table 2 suggest that the Babcock–Leighton mechanism is actually operating on the sun. Dasi-Espuig et al. [14] arrived at the same conclusion performing a quite different analysis of KK and MW data.

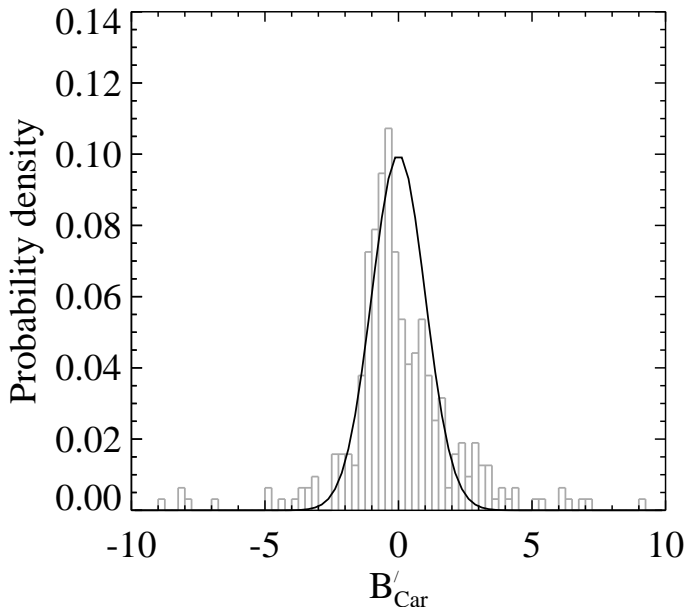


Fig. 3. Distribution of fluctuations  $B'_{Car}$  estimated from the CSA data.

Let us now consider fluctuations of the  $\alpha$ -effect for the Babcock–Leighton mechanism. Figure 3 shows the distribution of the (relative) fluctuations  $B'_{Car}$  (2) estimated from the CSA data. The distribution is close to normal. The relative amplitude (3) of the fluctuation is given in Table 3. We include fluctuations of the  $\alpha$ -effect with the estimated amplitude in the dynamo model described later.

Short-term fluctuations in solar-dynamo models are known to result in alternations of durable epochs of comparatively high and comparatively low amplitudes of magnetic cycles. The fluctuations could be responsible for the stochastic dynamics of the solar



activity on time scales of millennia [28].

### 3. GRAND MINIMA AND MAXIMA IN THE DYNAMO MODEL

#### 3.1. The Model

Our dynamo model is very close to that of an earlier paper [29]. The only difference is that fluctuations of the  $\alpha$ -effect are now allowed for. The allowance for the fluctuations will, therefore, be discussed in detail, while other features of the model are outlined briefly. All further details can be found in [29].

Our numerical model evolves the large-scale (longitude-averaged) magnetic field with time in the spherical shell of the convective zone. We assume axial symmetry of the field

$$\mathbf{B} = \mathbf{e}_\phi B + \text{rot} \left( \mathbf{e}_\phi \frac{\mathcal{A}}{r \sin \theta} \right), \quad (5)$$

where  $r$ ,  $\theta$ , and  $\phi$  are the usual spherical coordinates,  $\mathbf{e}_\phi$  is the azimuthal unit vector,  $B$  is the toroidal field, and  $\mathcal{A}$  is the poloidal field potential. A similar expression for the fluid velocity,

$$\mathbf{V} = \mathbf{e}_\phi r \sin \theta \Omega f(r, \theta) + \frac{1}{\rho} \text{rot} \left( \mathbf{e}_\phi \frac{\psi}{r \sin \theta} \right), \quad (6)$$

accounts for rotation and meridional circulation. In this equation,  $\Omega$  is the mean angular velocity,  $f$  is the dimensionless rotational frequency, and  $\psi$  is the stream function of the meridional flow. The differential rotation is prescribed in accordance with helioseismology and the meridional flow is specified in accordance with the model [30] for the global solar circulation.

Two specific properties of the model are the diamagnetic transport of the field with the effective velocity

$$\mathbf{U}_{\text{dia}} = -\frac{1}{2} \nabla \eta_{\text{T}} \quad (7)$$

[1], where  $\eta_{\text{T}}$  is the turbulent magnetic diffusivity, and non-local formulation of the  $\alpha$ -effect of the Babcock–Leighton type.

The dynamo equations are normalized to dimensionless variables. The equation for the toroidal field,

$$\begin{aligned} \frac{\partial B}{\partial t} &= \frac{\eta}{x^2} \frac{\partial}{\partial \theta} \left( \frac{1}{\sin \theta} \frac{\partial(\sin \theta B)}{\partial \theta} \right) + \frac{1}{x} \frac{\partial}{\partial x} \left( \sqrt{\eta} \frac{\partial(\sqrt{\eta} x B)}{\partial x} \right) + \\ &+ \frac{R_{\text{m}}}{x} \frac{\partial}{\partial \theta} \left( \frac{B}{\rho x \sin \theta} \frac{\partial \psi}{\partial x} \right) - \frac{R_{\text{m}}}{x} \frac{\partial}{\partial x} \left( \frac{B}{\rho x \sin \theta} \frac{\partial \psi}{\partial \theta} \right) + \end{aligned}$$

$$+ \frac{\mathcal{D}}{x} \left( \frac{\partial f}{\partial x} \frac{\partial \mathcal{A}}{\partial \theta} - \frac{\partial f}{\partial \theta} \frac{\partial \mathcal{A}}{\partial x} \right), \quad (8)$$

includes two governing parameters: the dynamo number,

$$\mathcal{D} = \frac{\alpha_0 \Omega R_\odot^3}{\eta_0^2} \quad (9)$$

and the magnetic Reynolds number for the meridional flow,

$$R_m = \frac{V_0 R_\odot}{\eta_0}. \quad (10)$$

Here,  $\alpha_0$  is the characteristic value of the  $\alpha$ -effect,  $\eta_0$  is the coefficient of turbulent diffusion at the middle of the convection zone, and  $V_0$  is the amplitude of the meridional velocity. The time  $t$  is measured in units of the diffusion time,  $R_\odot^2/\eta_0$ , and  $x = r/R_\odot$  is the relative radius.

All the computations were performed with the dynamo number  $\mathcal{D} = 4.2 \times 10^4$ , which slightly exceeds the critical value  $\mathcal{D}_{\text{cr}} = 3.96 \times 10^4$  for which the dynamo effect sets on. The Reynolds number  $R_m = 10$ , which corresponds to the amplitude of the meridional flow  $V_0 \simeq 14$  m/s, assuming  $\eta_0 \simeq 10^9$  m<sup>2</sup>/s.

The equation for the poloidal field,

$$\begin{aligned} \frac{\partial \mathcal{A}}{\partial t} &= \frac{\eta}{x^2} \sin \theta \frac{\partial}{\partial \theta} \left( \frac{1}{\sin \theta} \frac{\partial \mathcal{A}}{\partial \theta} \right) + \sqrt{\eta} \frac{\partial}{\partial x} \left( \sqrt{\eta} \frac{\partial \mathcal{A}}{\partial x} \right) + \\ &+ \frac{R_m}{\rho x^2 \sin \theta} \left( \frac{\partial \psi}{\partial x} \frac{\partial \mathcal{A}}{\partial \theta} - \frac{\partial \psi}{\partial \theta} \frac{\partial \mathcal{A}}{\partial x} \right) + \\ &+ (1 + s\sigma_{B_{\text{Car}}}) x \sin^3 \theta \cos \theta \int_{x_i}^x \alpha(x, x') B(x', \theta) dx', \end{aligned} \quad (11)$$

differs from that used earlier in [29] only by the presence of finite  $s\sigma_{B_{\text{Car}}}$  in its last term. The finite  $s\sigma_{B_{\text{Car}}}$  takes into account the fluctuations of the  $\alpha$ -effect. In Eq. (11),  $\sigma_{B_{\text{Car}}}$  is the relative magnitude of the fluctuations (3) and  $s$  is a random number with Gaussian distribution and rms value equal to one. The normal distribution for  $s$  was realized using the Box–Muller transformation [31]. The quantity  $s$  remains constant within the (dimensionless) time interval  $\tau = 5 \times 10^{-5}$ , which approximately corresponds to the period of solar rotation. After time  $\tau$  passed,  $s$  takes a new random value independent of its preceding value. This new value remains constant during time  $\tau$ , then is replaced by a new random value for a time  $\tau$ , and so on. Thus, the fluctuations of the  $\alpha$ -effect are modeled by a Poisson-type random process. This, however, does not mean that the

variations of amplitudes of the magnetic cycles also obey a Poisson distribution. The magnetic field varies continuously with time, and the dynamo memory-time significantly exceeds the correlation time for the random fluctuations in the  $\alpha$ -effect. The relative magnitude of the fluctuations of the  $\alpha$ -effect in the model is inferred from the CSA data,  $\sigma_{B_{\text{Car}}} = 2.67$  (see Table 2).

The function  $\alpha(x, x')$  in (11) characterizes the non-local properties of the  $\alpha$ -effect. Similar to [29], this function was taken in the form

$$\alpha(x, x') = \frac{\phi_b(x')\phi_\alpha(x)}{1 + B^2(x', \theta)}, \quad (12)$$

where  $B^2$  in the denominator accounts for the non-linear suppression of the  $\alpha$ -effect, the function  $\phi_b(x')$  defines a spherical layer near the base of the convective zone, whose toroidal field produces the  $\alpha$ -effect, and the function  $\phi_\alpha(x)$  defines the subsurface region in which this effect is produced. Figure 4 presents the functions  $\phi_b$  and  $\phi_\alpha(x)$ , together with the profile of the (normalized) magnetic diffusion  $\eta$  used in the dynamo model.

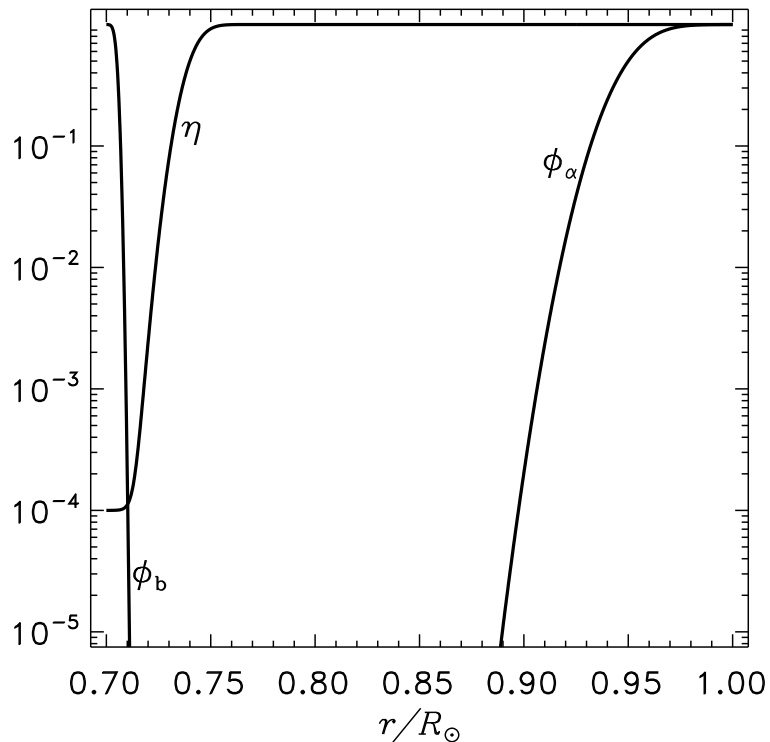


Fig. 4. The functions  $\phi_b$  and  $\phi_\alpha$  and the profile of the magnetic diffusion  $\eta$ .

The lower boundary is located at  $x_i = 0.7$ . The boundary conditions there correspond to the interface with a superconductor, while the vacuum conditions were imposed on the top boundary. We solved the dynamo equations (8) and (11) numerically applying an explicit finite-difference scheme.

Taking  $\sigma_{B_{\text{Cor}}} = 0$  in (11) eliminates fluctuations of the  $\alpha$ -effect, and the dynamo model becomes identical to that discussed in [29]. This model can reproduce the main features of the solar cycle fairly well. Here, we simulate global solar minima (and maxima) by including fluctuations in the Babcock–Leighton  $\alpha$ -effect.

It is believed that solar active regions emerge when deep toroidal fields rise to the solar surface. Within each cycle, then, the number of sunspots varies in phase with the toroidal field. Since the Babcock–Leighton mechanism is related to sunspot activity, we assume that the number of sunspots is proportional to the same magnetic flux of the toroidal field, which defines the  $\alpha$ -effect of the equations (11) and (12):

$$B_w = \int_{x_i}^1 \int_0^\pi \sin \theta x \phi_b(x) |B(x, \theta)| dx d\theta. \quad (13)$$

Here, the integrand in (13) contains the absolute value of  $B(x, \theta)$ , since the Wolf number is defined independent of sunspot polarity. The relationship between the Wolf number and  $B_w$  (13) is [32]

$$W = C_w B_w \exp\left(-\frac{B_0}{B_w}\right). \quad (14)$$

The parameter values  $C_w = 10^5$  and  $B_0 = 2 \times 10^{-5}$  provide the best agreement with the maximum and mean Wolf numbers reconstructed from the radiocarbon  $^{14}\text{C}$  content in natural archives [33] ([ftp://ftp.ncdc.noaa.gov/pub/data/paleo/climate\\_forcing/solar\\_variability](ftp://ftp.ncdc.noaa.gov/pub/data/paleo/climate_forcing/solar_variability)).

### 3.2. Grand Minima and Maxima

We computed the field evolution over a long-time interval, encompassing approximately 11 000 years in physical (dimensional) time. The model takes into account fluctuations of the  $\alpha$ -effect as described above. These fluctuations result in variations of the durations of the magnetic cycles, from about 7.3 to 15.1 years. The calculated amplitudes of the cycles also vary. Figure 5a shows the calculated magnetic flux (13) as a function of time. The narrow peaks in Fig. 5a correspond to individual magnetic cycles. We can see that epochs of higher magnetic activity alternate with epochs of weak magnetic fields.

To analyze the global minima and maxima of the dynamo model, the computed function  $B_w(t)$  was subject to a transformation following as closely as possible the processing applied to data on solar activity in the remote past [28]. We first convert  $B_w$

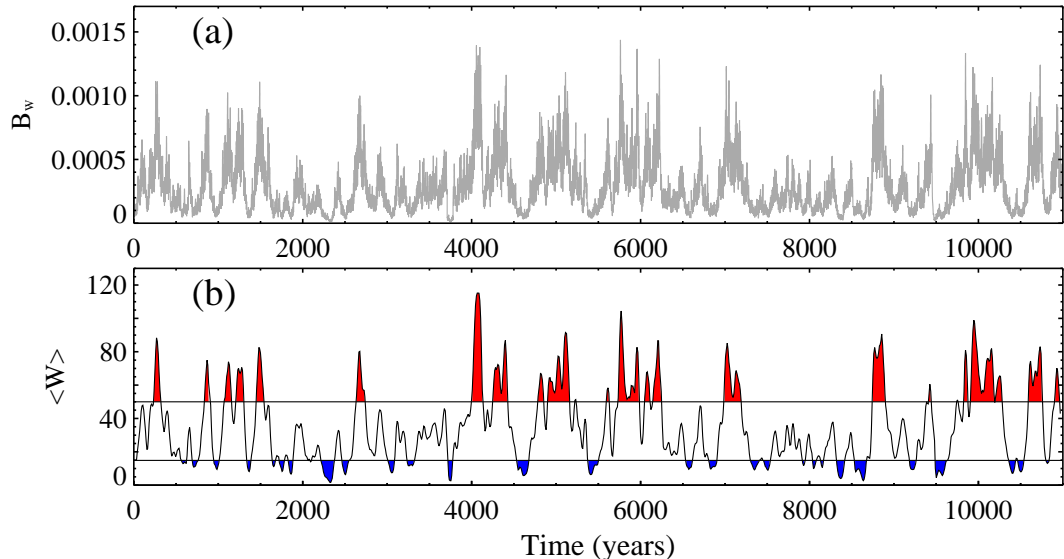


Fig. 5. The (a) magnetic flux  $B_w(t)$  and (b) smoothed amplitudes  $\langle W \rangle$  of the activity cycles as a function of time.

into sunspot numbers by Eq. (14). We then smooth the so defined "Wolf numbers" by computing its running mean over 13 solar rotations, i.e., over approximately one year. In analyses of long-term variations of solar activity, the cycle amplitude is usually defined as the maximum annual mean number of sunspots. Various smoothing techniques were applied formerly to reveal secular and super-secular variations, with Gleisberg secular smoothing [34] being used most frequently. Part (b) of Fig. 5 shows the cycle amplitude smoothed in this way as a function of time. The rules for identifying the grand minima and maxima are similar to those applied in [28] to solar data. An epoch is identified as a grand minimum if  $W$  was below 15 during at least two successive cycles ( $> 20$  yrs). If the interval between two neighboring minima was less than 30 yrs, such low-activity epochs were combined into a single global minimum. In turn, global maxima were defined as the epochs of  $W$  exceeding 50. Global minima and maxima are indicated by blue and red colours, respectively, in Fig. 5b and subsequent figures.

Figure 6a shows a histogram of the smoothed amplitudes of the magnetic cycles  $W$  (14). 22% of the calculated cycles have amplitudes  $< 15$  to belong to grand minima, while 25% with amplitudes  $> 50$  belong to grand maxima.

Figure 6b shows a histogram of durations of magnetic cycles. The mean cycle duration in our model is about ten years, somewhat shorter than the observed 11 years. The durations of the simulated cycles vary from 7.3 to 15.1 yrs, but 93% of the cycles lie within the range of 8–11.5 yrs. Shorter cycles dominate during epochs of grand minima.

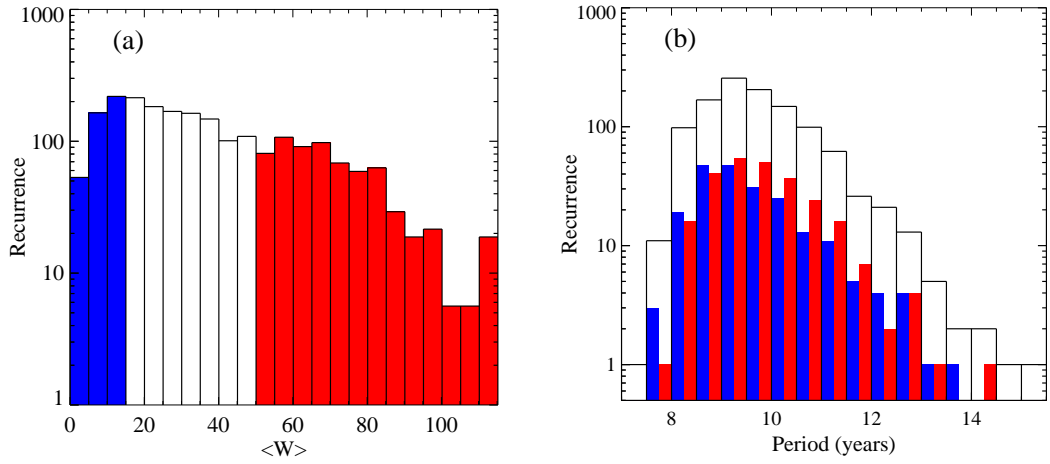


Fig. 6. Histograms of the (a) amplitudes and (b) durations of magnetic cycles. Blue and red correspond to the grand minima and grand maxima, respectively. Uncoloured histogram in part (b) shows total number of cycles disregarding their amplitudes.

According to Nesme-Ribes et al. [35], durations of the cycles that emerged at the end of the Maunder minimum were about 9–10 yrs. However, the variations in solar activity deduced from the content of cosmogenic isotopes in natural archives do not confirm this [36].

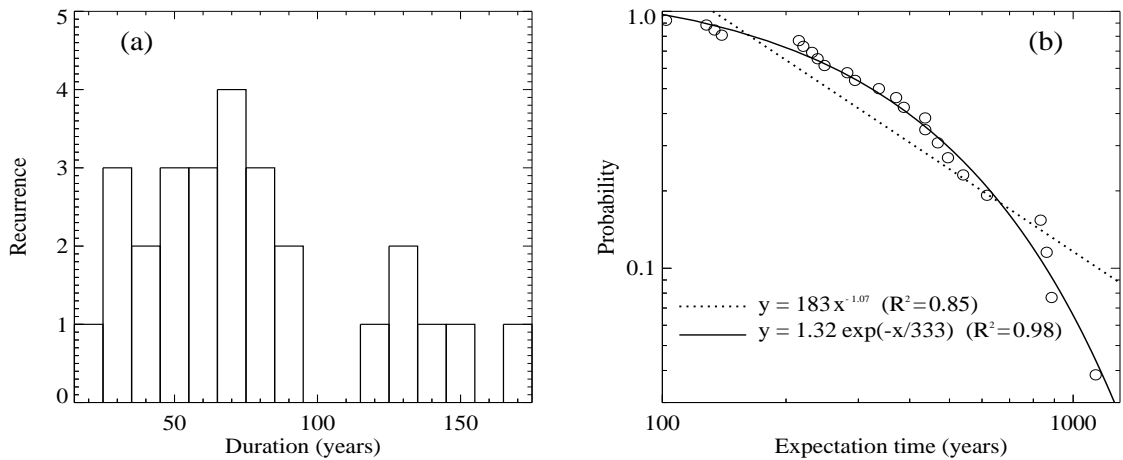


Fig. 7. (a) Histogram of the durations of the grand minima and (b) probability for the waiting time to be equal or longer than  $t$  as function of  $t$ .

Figure 7a shows the distribution of grand minima durations. We can find relatively short minima of 30 – 90 yrs (77.8%), as well as longer minima of  $> 110$  yrs (22.2%). Similar groups of grand minima were found from the cosmogenic isotopes data [28,37] and named the Maunder and Sперer type minima, respectively. In our computations, the total duration of the grand minima equals 2009 yrs, reaching 18.3% of the computation time. The computations show 27 grand minima.

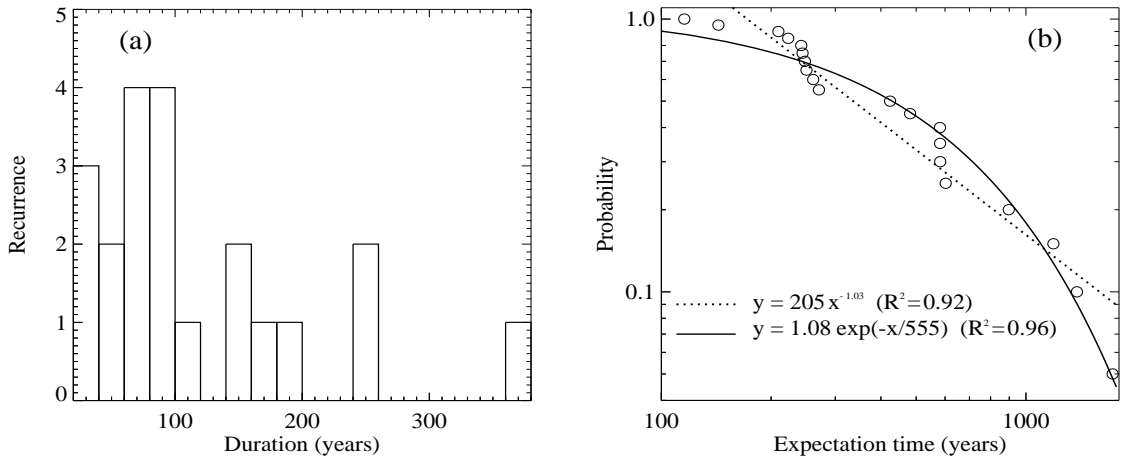


Fig. 8. Same as in Fig. 7 but for the grand maxima.

Another important feature of global minima (maxima) is their separation in time, called the waiting time [28]. The waiting time is defined as the time interval  $t$  between the centers of successive global minima or maxima. Figures 7b and 8b show the probabilities for the waiting time to be equal to or longer than  $t$  as a function of this  $t$ . For a finite number of observed or simulated events, this probability can be estimated as

$$y(t) = \frac{N(t)}{N(0)}, \quad (15)$$

where  $N(t)$  is the number of events with waiting times not smaller than  $t$ . We approximated the estimated probability distributions by exponential and power-law functions:

$$y(t) \propto \exp\left(\frac{-t}{T}\right) \quad (16)$$

or

$$y(t) \propto t^{-\gamma}. \quad (17)$$

The best-fit parameters we defined by the least-squares method. The exponential distribution (16) corresponds to the Poisson random process, in which each successive event occurs independently of preceding events. Such a process has no memory of preceding events.

Figure 7b shows the distribution of the waiting times for the grand minima. The parameter of the exponential fit  $T = 333 \pm 14$  yrs approximately corresponds to the mean waiting time. The exponential function describes the probability distribution better than the power law.

Figure 8 shows a histogram of the durations and the distribution of the waiting times for the grand maxima. Similar to the case of the grand minima, the distribution is close

to a Poisson random process. Analysis of the solar activity in the remote past leads to a similar conclusion [28]. Table 3 compares the observed and computed results in more detail.

Table 3. Model computations compared with the solar activity data for about 11 000 years [28]

Parameters	Model calculations	Solar data ( $^{14}\text{C}$ )
<b>Grand minima</b>		
Number	27	27
Total duration	2009 years	1880 years
	18%	17%
Mean duration	74 years	70 years
Waiting time	$T = 333 \pm 14$ years	$T = 435 \pm 15$ years
	$\Gamma = 1.07 \pm 0.09$	$\Gamma = 0.95 \pm 0.02$
<b>Grand maxima</b>		
Number	21	19, 22*
Total duration	2484 years	1030 years, 1560 years*
	23%	9%, 22%*
Waiting time	$T = 555 \pm 24$ years	$T = 355 \pm 20$ years
	$\Gamma = 1.03 \pm 0.07$	$\Gamma = 0.77 \pm 0.05$

\* Calculated using 7000 years long data series.

Though the fluctuations of the  $\alpha$ -effect in our model represent a Poisson-type random process, the nearly Poisson distribution found for the grand minima (and maxima) is not obvious. The magnetic field varies continuously in the dynamo process and undoubtedly "remembers" its preceding states. Nevertheless, random fluctuations in the  $\alpha$ -effect result in memory loss on time scales exceeding the cycle period.

Figure 9 shows time-latitude diagrams for the toroidal field at the base of the convective zone and for the radial field at the solar surface. The radial (poloidal) field demonstrates both regular variations in the dynamo cycles and irregular changes over shorter time scales comparable to the solar rotation period. The poloidal field is generated by the  $\alpha$ -effect, and its irregular changes are due to the random fluctuations in the  $\alpha$ -effect of our model. The toroidal field is generated by the (steady) differential rotation. Therefore, the deep toroidal field in Fig. 9 shows only almost periodic cycles with a slowly varying amplitude.

#### 4. CONCLUSIONS

The above estimates of the Babcock–Leighton mechanism based on data from three sunspot catalogs support the idea that this mechanism operates on the Sun. This mechanism for the generation of the poloidal field is a particular kind of the  $\alpha$ -effect of hydromag-



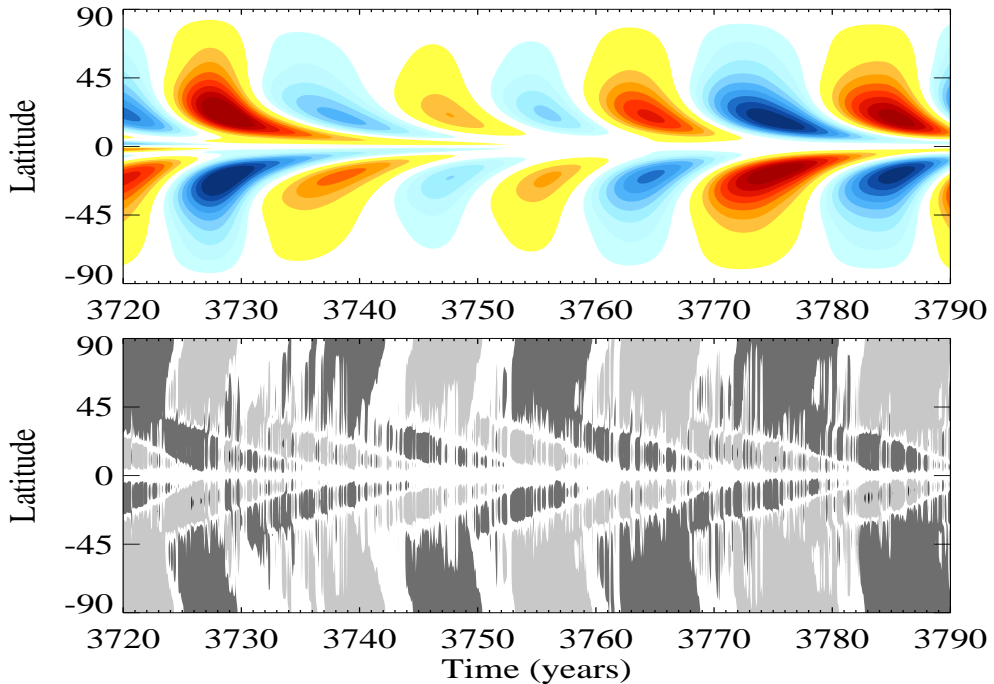


Fig. 9. Time-latitude diagrams for the toroidal field at the base of the convective zone (top panel) and the radial field at the surface (bottom). Yellow and red (blue) colours for toroidal field and dark (light) shading for the radial field correspond to positive (negative) sign of the fields.

netic dynamos. An important feature of the Babcock–Leighton  $\alpha$ -effect is its non-local character: the generation of the poloidal field near the solar surface is associated with the toroidal field located at the base of the convective zone. The non-local  $\alpha$ -effect enables us to improve the agreement between dynamo models and solar observations [29].

Our calculations show that taking into account fluctuations of the (non-local)  $\alpha$ -effect enables us to reproduce global changes in solar activity on time scales of centuries. Here, we have used fluctuation parameters estimated from sunspot data. The fluctuations in the Babcock–Leighton  $\alpha$ -effect are not small; their amplitude appreciably exceeds the mean value. These fluctuations occur on comparatively short time scales of the order of the solar rotation period. Our model calculations show that global changes in solar activity similar to the Maunder minimum can be caused by irregular variations in dynamo parameters on a time scale of the order of the solar rotation period.

Our proposed model takes into account only the rough characteristics of the fluctuations of the  $\alpha$ -effect. The model includes temporal fluctuations and neglects irregular spatial changes, which certainly are also present. Nevertheless, the parameters of the grand solar minima (maxima) calculated are in overall agreement with data on solar activity in the remote past (see Table 3). At the same time, the model proposed cannot reproduce fine

features of global changes, such as the breaking of the equatorial symmetry in solar activity as observed at the end of the Maunder minimum [38,39]. This effect requires accounting for irregular changes in the  $\alpha$ -effect with latitude, which can be a perspective for development of the model.

This work was supported by the Russian Foundation for Basic Research (projects 12-02-92691-IND\_a, 13-02-00277, and 12-02-33110- mol\_a\_ved) and the Ministry of Education and Science of the Russian Federation (state contract No 16.518.11.7065).

## REFERENCES

1. F. Krauze and K.-H. Rädler, *Mean Field Electrodynamics and Dynamo Theory* (Pergamon, Oxford, 1980; Mir, Moscow, 1984).
2. B. J. Labonte and R. Howard, *Sol. Phys.* **75**, 161 (1982).
3. S. V. Vorontsov, J. Christensen-Dalsgaard, J. Schou, *et al.*, *Science* **296**, 101 (2002).
4. V. I. Makarov and A. G. Tlatov, *Astron. Rep.* **44**, 759 (2000).
5. V. I. Makarov, A. G. Tlatov, D. K. Callebaut, *et al.*, *Sol. Phys.* **198** 409 (2001).
6. J. Jiang, P. Chatterjee, and A. R. Choudhuri, *MNRAS* **381**, 1527 (2007).
7. A. R. Choudhuri, *Proc. IAU Symp. 273 The Physics of Sun and Star Spots*. D. Choudhary & K. Strassmeier (eds.) Kluwer, Dordrecht, p.28 (2011).
8. E. N. Parker, *Astrophys. J.* **122**, 293 (1955).
9. H. W. Babcock, *Astrophys. J.* **133**, 572 (1961).
10. R. B. Leighton, *Astrophys. J.* **156**, 1 (1969).
11. L. L. Kitchatinov and S. V. Olemskoy, *Astron. Lett.* **37**, 286 (2011).
12. L. L. Kitchatinov and S. V. Olemskoy, *Astron. Nachr.* **332**, 496 (2011).
13. D. V. Erofeev, *Proc. IAU Symposium 223 Multi-Wavelength Investigations of Solar Activity*. A. V. Stepanov, E. E. Benevolenskaya & A. G. Kosovichev (eds.) Kluwer, Dordrecht, p.97 (2004).

14. M. Dasi-Espuig, S.K. Solanki, N.A. Krivova, *et al.*, *Astron. Astrophys.* **518** A7 (2010).
15. L.L. Kitchatinov and S.V. Olemskoy, *Astron. Lett.* **37**, 656 (2011).
16. S.H. Saar and S.L. Baliunas, *The Solar Cycle Workshop*. K.L. Harvey (ed.) ASP Conf. Series **27**, 150 (1992).
17. A.R. Choudhuri, *Astron. Astrophys.* **253**, 277 (1992).
18. A. J. H. Ossendrijver, P. Hoyng, and D. Schmitt, *Astron. Astrophys.* **313**, 938 (1996).
19. D. Moss, D. Sokoloff, I. Usoskin, and V. Tutubalin, *Sol. Phys.* **250**, 221 (2008).
20. I. G. Usoskin, D. Sokoloff, and D. Moss, *Sol. Phys.* **254**, 345 (2009).
21. M.S. Miesch, A.S. Brun, and J. Toomre, *Astrophys. J.* **641**, 618 (2006).
22. Y.-M. Wang and N.R. Sheeley Jr., *Sol. Phys.* **124**, 81 (1989).
23. V.N. Obridko, *Solar Spots and Activity Complexes* (Nauka, Moscow, 1985) [in Russian].
24. Yu.A. Nagovitsyn, E.V. Miletskii, V.G. Ivanov, and S.A. Guseva, *Kosmich. Issled.* **46**, 291 (2008).
25. R. Howard, P. I. Gilman, and P. A. Gilman, *Astrophys. J.* **283**, 373 (1984).
26. R. F. Howard, S. S. Gupta, and K. R. Sivaraman, *Sol. Phys.* **186**, 25 (1999).
27. A. R. Choudhuri, *J. Astrophys. Astr.* **29**, 41 (2008).
28. I. G. Usoskin, S. K. Solanki, and G. A. Kovaltsov, *Astron. Astrophys.* **471**, 301 (2007).
29. L. L. Kitchatinov and S. V. Olemskoy, *Sol. Phys.* **276** 3 (2012).
30. L. L. Kitchatinov and S. V. Olemskoy, *MNRAS* **411** 1059 (2011).
31. W. H. Press, S. A. Teukolsky, W. T. Vetterling, and B. P. Flannery, *Numerical Recipes*. Cambridge Univ. Press (1992).
32. V. V. Pipin, D. D. Sokolov, and I. G. Usoskin, *Astron. Astrophys.* **542**, A26 (2012).

33. S. K. Solanki, I. G. Usoskin, B. Kromer, et. al., *Nature* **431**, 1084 (2004).
34. Yu.I. Vitinskii, M. Kopetskii, and G.V. Kuklin, *Statistics of Spot-Forming Activity of the Sun* (Nauka, Moscow, 1986) [in Russian].
35. E. Nesme-Ribes, D. Sokoloff, J. C. Ribes, and M. Kremliovsky, in *The Solar Engine and its Influence on Terrestrial Atmosphere and Climate*. NATO ASI Ser., Vol. I 25, E. Nesme-Ribes (ed.) Springer, Berlin, p.71 (1994).
36. K. Nagaya, K. Kitazawa, F. Miyake, et al., *Sol. Phys.* **280**, 223 (2012).
37. M. Stuiver and T. F. Braziunas, *Nature* **338**, 405 (1989).
38. D. Sokoloff and E. Nesme-Ribes, *Astron. Astrophys.* **288**, 293 (1994).
39. R. Arlt, *Sol. Phys.* **255**, 143 (2009).